Key Points:
- Combined $[CO_3^{2-}]$, $\delta^{13}C$, and U/Ca_C evidence indicates increased respired carbon storage in the Last Glacial Maximum Eastern Equatorial Pacific
- Along with reduced deep water ventilation, this evidence points to enhanced soft-tissue pump efficiency driven by ocean circulation changes
- Modest $[CO_3^{2-}]$ change suggests calcite dissolution as a further contribution to atmospheric CO_2 drawdown via increased ocean alkalinity

Supporting Information:
- Supporting Information S1
- Tables S1–S4

Correspondence to:
M. de la Fuente,
md717@cam.ac.uk

The Evolution of Deep Ocean Chemistry and Respired Carbon in the Eastern Equatorial Pacific Over the Last Deglaciation

Maria de la Fuente[1,2] (iD), Eva Calvo[1] (iD), Luke Skinner[2], Carles Pelejero[1,3] (iD), David Evans[4] (iD), Wolfgang Müller[5,6], Patricia Povea[7], and Isabel Cacho[7] (iD)

[1]Institut de Ciències del Mar, CSIC, Barcelona, Spain, [2]Godwin Laboratory for Palaeoclimate Research, Department of Earth Sciences, University of Cambridge, Cambridge, UK, [3]Institució Catalana de Recerca i Estudis Avançats, Barcelona, Spain, [4]School of Earth and Environmental Sciences, University of St Andrews, St Andrews, UK, [5]Department of Earth Sciences, Royal Holloway, University of London, London, UK, [6]Institute of Geosciences, Goethe-Universität Frankfurt, Frankfurt, Germany, [7]Grup de Recerca Consolidat en Geociències Marines, Departament de Dinàmica de la Terra i de l'Oceà, Universitat de Barcelona, Barcelona, Spain

Abstract It has been shown that the deep Eastern Equatorial Pacific (EEP) region was poorly ventilated during the Last Glacial Maximum (LGM) relative to Holocene values. This finding suggests a more efficient biological pump, which indirectly supports the idea of increased carbon storage in the deep ocean contributing to lower atmospheric CO_2 during the last glacial. However, proxies related to respired carbon are needed in order to directly test this proposition. Here we present *Cibicides wuellerstorfi* B/Ca ratios from Ocean Drilling Program Site 1240 measured by laser ablation inductively coupled plasma mass spectrometry (LA-ICPMS) as a proxy for deep water carbonate saturation state ($\Delta[CO_3^{2-}]$, and therefore $[CO_3^{2-}]$), along with $\delta^{13}C$ measurements. In addition, the U/Ca ratio in foraminiferal coatings has been analyzed as an indicator of oxygenation changes. Our results show lower $[CO_3^{2-}]$, $\delta^{13}C$, and $[O_2]$ values during the LGM, which would be consistent with higher respired carbon levels in the deep EEP driven, at least in part, by reduced deep water ventilation. However, the difference between LGM and Holocene $[CO_3^{2-}]$ observed at our site is relatively small, in accordance with other records from across the Pacific, suggesting that a "counteracting" mechanism, such as seafloor carbonate dissolution, also played a role. If so, this mechanism would have increased average ocean alkalinity, allowing even more atmospheric CO_2 to be "sequestered" by the ocean. Therefore, the deep Pacific Ocean very likely stored a significant amount of atmospheric CO_2 during the LGM, specifically due to a more efficient biological carbon pump and also an increase in average ocean alkalinity.

1. Introduction

Several marine carbon cycle mechanisms have been invoked to explain, at least, a major part of the atmospheric CO_2 drawdown observed over the last glacial period (e.g., Kohfeld & Ridgwell, 2009; Sigman et al., 2010). These mechanisms can be categorized broadly as deriving primarily from (1) changes in whole ocean carbonate chemistry through global alkalinity (ALK) increase, for example, due to "carbonate compensation" or carbonate dissolution (e.g., Archer & Maier-Reimer, 1994); (2) changes in the conditions or efficiency of air-sea gas exchange, that is, changes in the "solubility pump" (e.g., Volk & Hoffert, 1985); or (3) changes in the accumulation of respired organic carbon (in the form of dissolved inorganic carbon, DIC) in the ocean interior, that is, changes in the global average efficiency of the "soft-tissue" component of the "biological carbon pump" (e.g., Volk & Hoffert, 1985), either in absolute terms or relative to the global average efficiency of its "carbonate pump" counterpart.

The efficiency of the soft tissue carbon pump was initially defined in terms of the gradient of major nutrient concentrations between the deep ocean and the shallow ocean, which arises due to the interplay of biological export from the surface ocean and the large-scale overturning circulation (Volk & Hoffert, 1985). Due to the association of carbon with biologically fixed nutrients, the efficiency of the soft tissue pump relates directly to the DIC concentration gradient between the surface and deep ocean (note that the two may become uncoupled due to air-sea gas exchange effects, which affect carbon but not major nutrients). A more efficient glacial soft-tissue pump would therefore result in greater carbon storage in the deep sea and a lower surface ocean and atmospheric pCO_2. This would occur as long as the soft-tissue pump remained dominant over its carbonate pump counterpart (as it is in the modern ocean), as an efficient carbonate pump draws

down surface ocean alkalinity and thus increases atmospheric CO_2. Changes in the relative strength of the soft tissue and carbonate pumps would be driven by, for example, biological community structure driven DIC:ALK "rain ratio" changes or water column remineralization profile changes (Archer & Maier-Reimer, 1994; Kwon et al., 2009). Notably, a global average increase in soft-tissue pump efficiency can occur as a result of (1) an increase in the biological flux of nutrients and carbon from the surface ocean to the deep interior, representing increased soft-tissue pump "strength" (e.g., Martínez-Garcia et al., 2014), and/or (2) a reduction in the return flux of remineralized nutrients and respired carbon from the deep interior to the surface ocean, for instance, due to a weaker large-scale overturning circulation, representing reduced soft-tissue pump "leakiness" (e.g., Stephens & Keeling, 2000; Toggweiler, 1999).

While a categorization of the various mechanisms for atmospheric CO_2 drawdown, as proposed above, might be useful for organizing our thinking about past marine carbon cycle changes, it is important to emphasize that these mechanisms need not have operated in isolation from each other. For example, if an increase in soft-tissue pump global efficiency was achieved via a change in ocean circulation, this would very likely co-occur with a change in the conditions of air-sea gas exchange and therefore the solubility pump. Furthermore, regardless of whether enhanced soft-tissue pump global efficiency is achieved via an increase in biological export rates or a reduction in the overturning circulation rate, it would lead to more respired carbon storage in the deep ocean, which in turn would lower deep ocean carbonate ion concentration ($[CO_3^{2-}]$), and $[O_2]$. If $[CO_3^{2-}]$ was reduced enough to cause seafloor carbonate dissolution (a mechanism also referred to as "respiratory calcite dissolution" (Archer, 1991, 1996; Archer & Maier-Reimer, 1994)), it would eventually increase the whole ocean alkalinity budget and lead to further atmospheric CO_2 drawdown.

It has been proposed that increased export production in the EEP over the last glacial period played a role storing more respired carbon in the deep ocean than during the Holocene (e.g., Doss & Marchitto, 2013; Pichevin et al., 2009; Robinson et al., 2009). However, other studies have argued against this (e.g., Costa et al., 2016; Winckler et al., 2016). Glacial $[O_2]$ decrease in the deep EEP supports higher respired DIC accumulation (Bradtmiller et al., 2010), although without elucidating the mechanism behind its variation. In this respect, it is now apparent that the EEP was less ventilated over the last part of the last glacial period, becoming better ventilated at the onset of the Heinrich Stadial 1 (de la Fuente et al., 2015; Umling & Thunell, 2017). This would indirectly support the idea of a more efficient biological pump during the last glacial due to a longer residence time for carbon in the deep ocean, thus reducing the leakiness of the biological pump and enhancing the deep ocean's respired carbon inventory.

In this study we set out to test the proposition that the respired carbon content of deep waters was indeed greater in the EEP during the LGM, as suggested by radiocarbon ventilation ages from this area (e.g., de la Fuente et al., 2015). Our approach is to combine several respired carbon-related proxies in the same sediment core Ocean Drilling Program (ODP) Site 1240 (hereafter referred to as ODP1240). Thus, measurements of $\delta^{13}C$ and B/Ca have been performed on the calcite shells of the benthic foraminifer species *Cibicides wuellerstorfi* as a means of reconstructing respired nutrient and $[CO_3^{2-}]$ changes, respectively. B/Ca analyses have been proposed as a method for reconstructing past deep water $[CO_3^{2-}]$ changes on the basis of an empirical correlation with deep water carbonate saturation state ($\Delta[CO_3^{2-}]$) (Yu & Elderfield, 2007), and on the assumption of invariant local saturation $[CO_3^{2-}]$ ($[CO_3^{2-}]_{sat}$). In addition, sedimentary redox conditions (i.e., estimates of changing $[O_2]$) have been reconstructed from analyses of U/Ca in the coatings (U/Ca$_C$; (Boiteau et al., 2012; Gottschalk et al., 2016)) of the planktonic species *Neogloboquadrina dutertrei* and have been compared to existing authigenic uranium (aU; (Bradtmiller et al., 2010; Cochran et al., 1986; Jaccard et al., 2016)) measurements from the same area (Bradtmiller et al., 2010; Kienast et al., 2007). Neither U/Ca$_C$ nor aU has so far been shown to quantify changes in O_2, and despite the fact that each of these approaches has its own limitations, we propose that their combination may offer robust qualitative information on glacial-interglacial bottom water/pore water $[O_2]$ changes.

2. Materials and Methods

2.1. EEP Hydrographic Settings

Sediment core ODP1240 was recovered from the southern edge of the Panama Basin in the EEP (0°01.31′N, 86°27.76′W) at 2,921 m water depth (Figure 1). The chronostratigraphy for this sediment core was previously
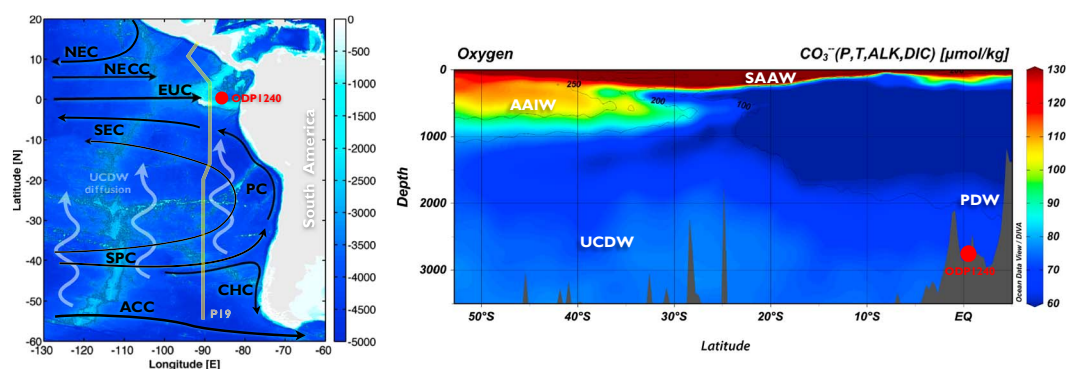
Figure 1. EEP hydrography. (left) The map of the study area displaying the bathymetry (blue scale), the location of the sediment core ODP1240 (red dot), the WOCE P19 transect (light yellow meridional line), and a scheme of the upper (black arrows) and deep (purple arrows) ocean circulation of the area: North Equatorial Current (NEC), North Equatorial Countercurrent (NECC), Equatorial Undercurrent (EUC), South Equatorial Current (SEC), Peru Current (PC), South Pacific Current (SPC), Cape Horn Current (CHC), Antarctic Circumpolar Current (ACC), and the northward diffusion of the Upper Circumpolar Deep Water mass (UCDW). (right) The vertical section of the WOCE P19 transect showing modern $[CO_3^{2-}]$ (color scale) and oxygen (contours) (Schlitzer, 2017). Water masses are indicated: Antarctic Intermediate Water (AAIW), UCDW, Subantarctic Water (SAAW), and Pacific Deep Water (PDW).

described by de la Fuente et al. (2015) and is based on sediment depth-age modeling using calibrated radiocarbon dates on *Neogloboquadrina dutertrei* that have been corrected for a variable reservoir age offsets, constrained through stratigraphic alignment of the $U_{37}^{K'}$ record from ODP1240 with Greenland $\delta^{18}O$ records. The hydrography of the EEP, in common with the whole tropical Pacific, is highly influenced by Southern Ocean water masses at depth (Kessler, 2006; Strub et al., 1998), with the depth of ODP1240 location, in particular, currently bathed by a mixture of Upper Circumpolar Deep Water (UCDW) and Pacific Deep Water (PDW; Figure 1). PDW refers to the water mass formed at depth in the North Pacific through very slow vertical mixing of bottom and intermediate waters of southern origin and extremely long residence times, and UCDW represents the upper layer of the deep water mass flowing within the Antarctic Circumpolar Current (ACC), a mixture of deep and recirculated waters from the Atlantic, Indian, and Southern Oceans (Mantyla & Reid, 1983; You, 2000). Although these deep water masses have different origins, both occupy approximately the same density and depth range in the Pacific (Talley et al., 2011) as a consequence of the extremely weak deep circulation in the Pacific Ocean. An additional feature of the modern Panama Basin hydrography is a degree of "biogeochemical aging" in its deepest part. Although this points to the possibility of highly localized influences on respired carbon in the Panama Basin, such influences do not affect the basin as a whole and are relatively small, with hardly any influence at the location of ODP1240 today.

2.2. B/Ca Analysis by LA-ICPMS and $[CO_3^{2-}]$ Estimates

The epibenthic foraminifer *C. wuellerstorfi* was picked from 15 samples from the top 3 m of sediment core ODP1240 covering the last ~30 kyr. Each sample was composed of approximately six specimens (>212 μm) that were rinsed in milliQ water and secured on a double-sided carbon tape on a glass slide for LA-ICPMS analysis. Between two and three depth-profiling ablations were made per shell using the RESOlution M-50 prototype 193 nm ArF laser ablation system (featuring a two-volume Laurin LA cell) coupled to an Agilent 7500ce quadrupole ICP-MS at Royal Holloway University of London (Müller et al., 2009). Ablation was performed using a laser spot size of 96 μm, repetition rate of 2 Hz, and fluence of ~4 J/cm². Data quantification follows Longerich et al. (1996) with the transformation of raw count rates to concentration achieved using ^{43}Ca as an internal standard and NIST610/612 as a calibration standard. The accuracy and precision of B/Ca measurements using these conditions is <5 and <10%, respectively (see Evans et al., 2015). Several steps to exclude any possible contaminant phases from the data were applied (Bolton et al., 2011; Boyle, 1983; Marr et al., 2011), and spots with B/Ca values higher than the individual foraminifer average plus 2SD were removed and not included in further palaeoclimatic interpretations. A more detailed discussion of

the methodology can be found in the supporting information (Eggins et al., 1998; Jochum et al., 2006; Jochum et al., 2011; Evans & Müller, 2013; Müller & Fietzke, 2016).

C. wuellerstorfi B/Ca ratios have been experimentally shown to linearly relate to $\Delta[CO_3^{2-}]$ based on global core top measurements in the modern ocean, as described by equation (1) below (Yu & Elderfield, 2007), thereby allowing downcore $[CO_3^{2-}]$ to be estimated from equation (2), albeit with some caution.

$$\Delta[CO_3^{2-}] = (B/Ca–177.1)/1.14 \text{ (in } \mu mol/mol) \tag{1}$$

$$\Delta[CO_3^{2-}] = [CO_3^{2-}] – [CO_3^{2-}]_{sat} \tag{2}$$

Seawater $[CO_3^{2-}]_{sat}$ in the modern ocean is estimated from water column $[CO_3^{2-}]/\Omega_{calcite}$ data, where $\Omega_{calcite}$ is the calcite saturation state in seawater ($\Omega_{calcite} = [Ca^{2+}] \cdot [CO_3^{2-}]/K_{sp}$, and K_{sp} is the solubility product of calcite ($[Ca^{2+}]_{sat} \cdot [CO_3^{2-}]_{sat}$) at a given temperature, salinity, and pressure). However, seawater $[CO_3^{2-}]_{sat}$ in the deep ocean is typically assumed to have remained constant over the late Pleistocene since the influence of pressure, bottom water temperature, and salinity in the past are thought to have exerted little effect on $[CO_3^{2-}]_{sat}$ over this time period (Allen et al., 2015). Thus, the general equation to estimate downcore $[CO_3^{2-}]$ through B/Ca ratios measured in the calcite shell of *C. wuellerstorfi* would be

$$[CO_3^{2-}] = ((B/Ca–177.1)/1.14) + \left([CO_3^{2-}]_{(mod)}/\Omega_{calcite\,(mod)}\right) \tag{3}$$

In this study, modern $[CO_3^{2-}]$ and $\Omega_{calcite}$ have been inferred from instrumental measurements of ALK and DIC available from the GLODAP data set (WOCE P19C transect; Tsuchiya & Talley, 1998). For these estimates, the CO2SYS software package (Lewis et al., 1998; Pierrot et al., 2006) and the equilibrium constants from Mehrbach et al. (1973) and Dickson and Millero (1987) were used. The obtained modern values at a depth of 2,888 m were 67.7 $\mu mol/kg$ for $[CO_3^{2-}]$ and 0.9 for $\Omega_{calcite}$, leading to a modern $[CO_3^{2-}]_{sat}$ of 75.2 $\mu mol/kg$ (station: 18373; LAT: 0.004°N; LONG: 85.84°W).

Since the initial calibration of Yu and Elderfield (2007) was published, several studies have provided additional core top measurements, but only one provided B/Ca results analyzed by LA-ICPMS (Raitzsch et al., 2011). In order to add further support to this technique, B/Ca ratios in *C. wuellerstorfi* specimens have been analyzed here in nine core top samples across the Atlantic Ocean by LA-ICPMS, following the same scheme described above for downcore analyses. Estimates of modern $\Delta[CO_3^{2-}]$ were obtained using either in situ data from the corresponding cruises when available, or data from nearby GLODAP sites (Key et al., 2004), in both cases by deriving values for modern $[CO_3^{2-}]$ and $\Omega_{calcite}$ (Table S1 in the supporting information).

2.3. $\delta^{13}C$ Measurements

Downcore $\delta^{13}C$ measurements were performed on 46 samples from ODP1240, covering the last 25 kyr and consisting exclusively of *C. wuellerstorfi* individuals from the >212 μm fraction size. The analyses were performed using a Thermo Kiel device attached to a Thermo MAT253 Mass Spectrometer in dual inlet mode at the University of Cambridge. The sample size was ~100 μg, with the exception of a few samples of 20 μg, which is close to the detection limit of this machine. A few additional $\delta^{13}C$ measurements in *C. wuellerstorfi* from ODP1240, consisting of four to five specimens each (also from the >212 μm size fraction) were obtained at the Scientific and Technological Center of the University of Barcelona (CCiT-UB) by using a FinniganMAT252 mass spectrometer fitted with a Kiel Carbonate Device I. All $\delta^{13}C$ values presented here are reported as per mil relative to the international standard Vienna Pee Dee Belemnite (VPDB), with a typical external reproducibility estimated to be equal or better than ±0.06‰ and ±0.03‰ for the Universities of Cambridge and Barcelona, respectively.

2.4. U/Ca Analysis in Planktonic Foraminiferal Coatings

U/Ca ratios measured in the foraminiferal shell coatings have been suggested to reflect changes in the sedimentary redox conditions and therefore potentially linked with changes in the $[O_2]$ in bottom waters (Boiteau et al., 2012). This oxygen-related proxy is based on the redox chemistry of U in seawater, shifting from the soluble form U(VI) in oxygenated waters to the insoluble U(IV) species as the medium depletes in oxygen (Cochran et al., 1986; Langmuir, 1978; Morford & Emerson, 1999).
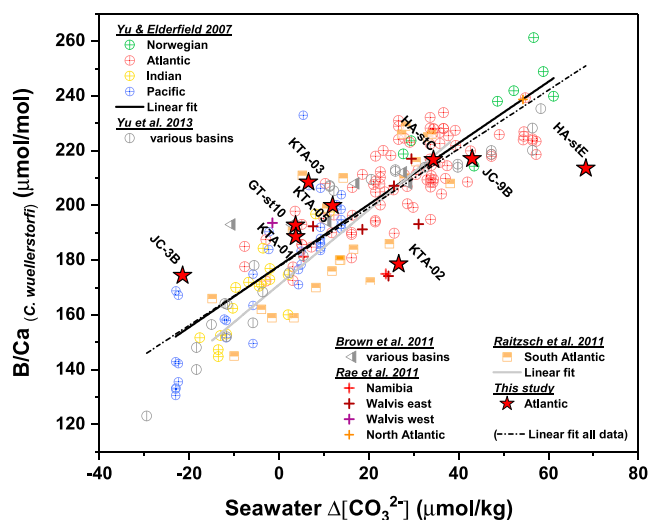
Figure 2. Bottom water $\Delta[CO_3^{2-}]$ versus B/Ca ratios in *C. wuellerstorfi* from core top samples analyzed by solution-ICPMS (Brown et al., 2011; Rae et al., 2011; Yu et al., 2013; Yu & Elderfield, 2007) and by LA-ICPMS (Raitzsch et al., 2011 and core tops from the Atlantic Ocean analyzed in this study (red stars)). Black solid line represents the linear fit from Yu and Elderfield (2007) by solution-ICP-MS, while gray solid line represents the linear fit from Raitzsch et al. (2011) by LA-ICP-MS. Black dashed line represent the linear fit from all the records together including the core tops analyzed in this study.

In order to quantify the U concentration in the foraminiferal coatings, clays were removed and an acid leach step to remove any adsorbed ions was performed in 20 *N. dutertrei* samples, each one composed of ~30 specimens collected from the 212–300 μm fraction. No oxidative or reductive step was performed in order to preserve the thin coating layer (Boiteau et al., 2012). Cleaned samples were dissolved in 0.1 M HNO_3, diluted to 10 ppm Ca^{2+}, and analyzed by ICP-MS at the University of Cambridge using a Thermo Element XR, with a typical analytical reproducibility of ~7%.

3. Results

3.1. *C. wuellerstorfi* B/Ca Core Top Measurements by LA-ICPMS

In Figure 2, *C. wuellerstorfi* B/Ca analyses from the Atlantic Ocean core tops are compared to their corresponding $\Delta[CO_3^{2-}]$ values, as well as to other core top data available from the literature (Brown et al., 2011; Rae et al., 2011; Raitzsch et al., 2011; Yu et al., 2013; Yu & Elderfield, 2007).

The core top measurements presented here (Table S1 in the supporting information) fit well within the two existing linear regressions from Yu and Elderfield (2007) ($A = 1.14$; $B = 177.1$) and from Raitzsch et al. (2011) ($A = 1.37$; $B = 170.9$), and combining all of the data results in an indistinguishable new calibration equation (~230 core top samples including this study; $A = 1.07$; $B = 177.7$), thus providing support for B/Ca as a proxy for $\Delta[CO_3^{2-}]$ and for LA-ICPMS as a suitable technique for this type of analysis. The original calibration equation from Yu and Elderfield (2007) is adopted here for downcore $\Delta[CO_3^{2-}]$ estimates in ODP1240 for better comparison with previously published data.

3.2. B/Ca-[CO$_3^{2-}$], $\delta^{13}C$, and U/Ca$_c$ Downcore ODP1240

Downcore B/Ca ratios from *C. wuellerstorfi* at ODP1240 are ~10 μmol/mol lower over the end of the last glacial period (~18–23 kyr), with an average of ~172 ± 5 μmol/mol (±1 SE), than across the late Holocene (~0–8 kyr), which exhibits values of ~182 ± 4 μmol/mol (±1SE) (Figure 3a). When converted into $[CO_3^{2-}]$ the difference between glacial (~71 μmol/kg) and interglacial (~80 μmol/kg) is ~9 μmol/kg, which is not as large as might be expected based on observed radiocarbon ventilation changes, possibly as a result of other processes that we discuss in the next sections. *C. wuellerstorfi* $\delta^{13}C$ measurements from ODP1240 are also characterized by lower values during the LGM compared to the Holocene of ~0.4‰, showing good consistency between measurements performed in the two laboratories (Figure 3b). Although both $[CO_3^{2-}]$ and $\delta^{13}C$ seem to be in good agreement and exhibit a similar pattern across the deglaciation, a "bump" just before the termination onset is observed only in the $[CO_3^{2-}]$ record. This may reflect processes that have an impact exclusively in $[CO_3^{2-}]$ without modifying $\delta^{13}C$ (i.e., changes in seafloor carbonate dissolution), or analysis artifacts in those specific samples. Although we cannot discard any of these possibilities unequivocally, the observed change in $[CO_3^{2-}]$ before the deglaciation seems to be too rapid to be explained by variations in calcite dissolution. U/Ca$_C$ measurements in the planktonic species *N. dutertrei* show higher values at the LGM compared to the Holocene suggesting, very likely, a more reducing environment at the water-sediment boundary at that time, and therefore lower $[O_2]$, in the deep EEP (Figure 3c). All data can be found in Tables S2, S3 and S4 in the supporting information.

4. Discussion

4.1. A Comparison of Ocean Ventilation and Carbonate System Changes in the EEP Across the Last Deglaciation

A poorly ventilated deep EEP at the end of the last glacial period compared to the present has been shown by the radiocarbon offsets between benthic foraminifera and atmospheric records (B-Atm) (de la Fuente et al., 2015). This study also revealed that better ventilation of this area of the Pacific began at the onset of the
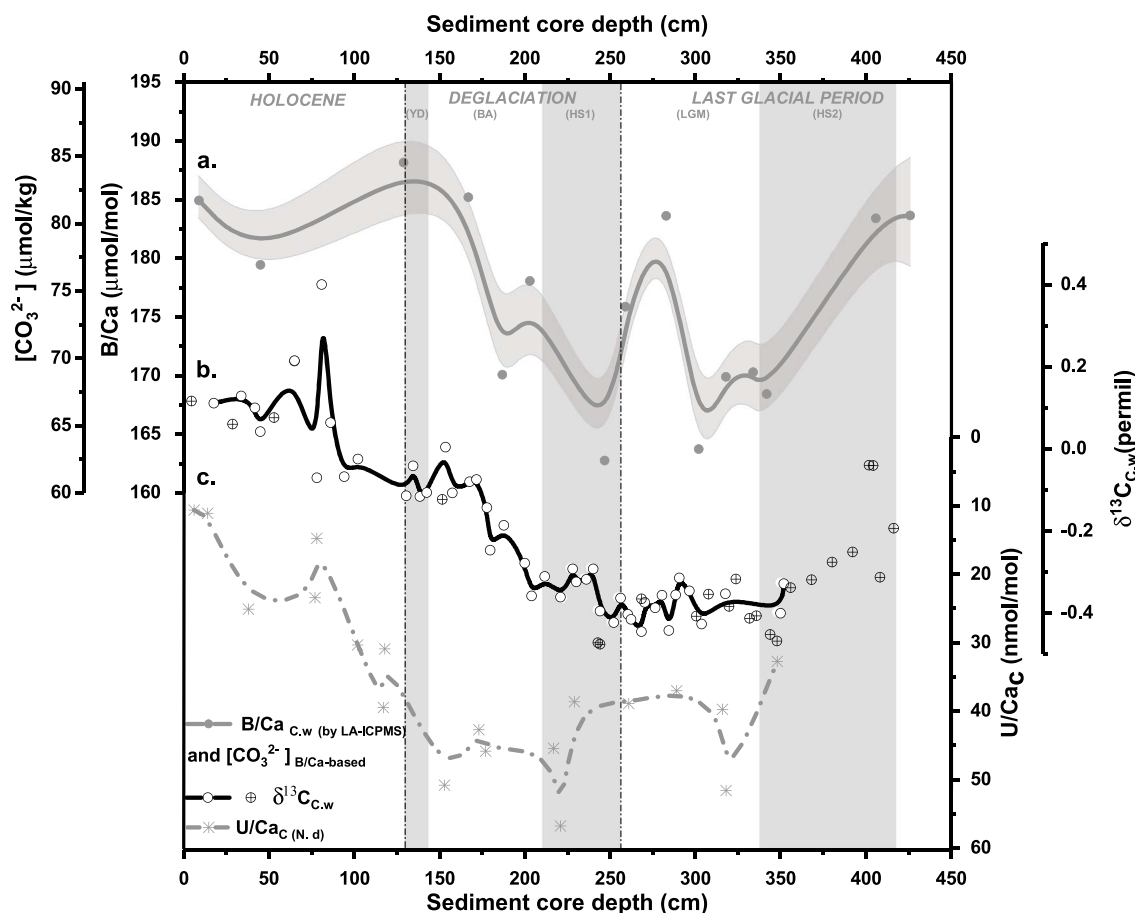
Figure 3. Deep water respired carbon related records across the first 450 cm of the sediment core ODP1240 (last ~30 kyr). (a) B/Ca ratios in *C. wuellerstorfi* measured by LA-ICP-MS and [CO_3^{2-}]-derived estimates (gray solid line/dots). Uncertainties represent ±1 SE in [CO_3^{2-}] (gray envelope). [CO_3^{2-}] was estimated by using the calibration equation from Yu and Elderfield (2007) and assuming a constant [CO_3^{2-}]$_{sat}$ value of 75.2 µmol/kg (estimated from modern [CO_3^{2-}] and $\Omega_{Calcite}$ values from the GLODAP data set WOCE P19 transect, see main text). (b) Benthic δ^{13}C from *C. wuellerstorfi* (black line/solid dots and crossed dots analyzed at the Universities of Cambridge and Barcelona, respectively). (c) U/Ca ratios in the coatings of *N. dutertrei* (gray dashed line/asterisks). All lines are B-spline smoothed. Vertical dashed lines delimit relevant climatic periods, and light gray vertical bands highlight the coldest periods of the last 30 kyr. HS1 and HS2: Heinrich Stadial 1 and 2 respectively; BA: Bølling-Allerød; YD: Younger Dryas.

deglaciation (~17.5 kyr B.P.), demonstrating a consistency with other ventilation records from the South Pacific (Siani et al., 2013; Sikes et al., 2000; Skinner et al., 2015) and the Atlantic sector of the Southern Ocean (Burke & Robinson, 2012; Skinner et al., 2010), all of which broadly covaried in time with changes in atmospheric Δ^{14}C and CO_2. Thus, when CO_2 increased and Δ^{14}C decreased in the atmosphere at the deglaciation onset (Figures 4a and 4b, respectively), all of these deep water ventilation records start to exhibit enhanced ventilation (Figure 4c, de la Fuente et al., 2015, and figures therein). This observation has at least two important implications: (1) that the deglacial increase in atmospheric CO_2 might be directly and causally linked to the deglacial evolution of deep ocean ventilation and (2) that the deep ocean, including the EEP, might have contained a higher concentration of respired CO_2 during the glaciation as compared to the late Holocene and thus acted as a source of carbon to the atmosphere during deglaciation.

In the absence of major ocean interior carbon sources, radiocarbon behaves as a semiconservative tracer that is not significantly affected by biological or chemical reactions within the ocean and tracks the mean time since a water mass exchanged carbon with the atmosphere. Radiocarbon ventilation estimates therefore allow us to isolate the contribution of ocean ventilation to changes in the global average efficiency of the soft-tissue pump. Increased radiocarbon ventilation ages observed in ODP1240 during the last late glacial period could therefore imply an increase in the amount of remineralised/oxidized organic matter in the ocean interior, that is, more carbon respired by microorganisms per unit volume due to more time
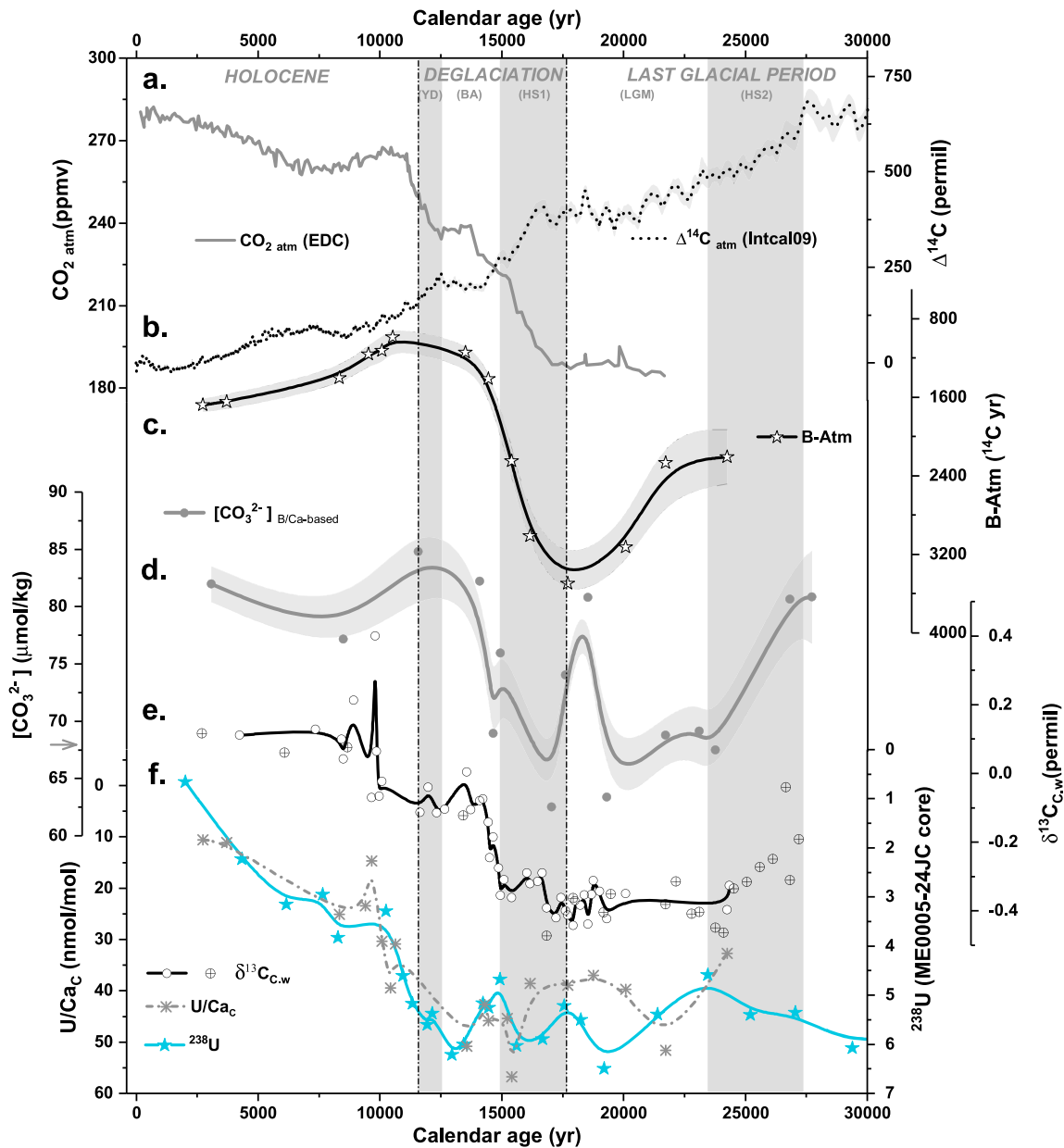
Figure 4. Comparison of deep ocean records from ODP1240 with records of atmospheric CO_2 and radiocarbon activity over the last 30 kyr. (a) Atmospheric CO_2 concentrations from EPICA Dome C (EDC) ice core (for the deglacial period, Monnin et al., 2001; for the Holocene period, Flückiger et al., 2002), placed on the age scale of Lemieux-Dudon et al. (2010) (gray line). (b) Atmospheric radiocarbon activity ($\Delta^{14}C$) changes (IntCal09 calibration curve; Reimer et al., 2009 (black dotted line). (c) Deep water ventilation reconstruction (B-Atm, from SST alignment in de la Fuente et al., 2015) (black line/white stars). (d) $[CO_3^{2-}]_{(B/Ca\text{-based})}$ (±SE) (gray solid line/dots). (e) $\delta^{13}C$ from *C. wuellerstorfi* (black line/solid dots and crossed dots analyzed at the Universities of Cambridge and Barcelona, respectively). (f) Oxygenation proxies: U/Ca_C from *N. dutertrei* (gray dashed line/asterisks) and ^{238}U from ME0005-24JC (same location as Site 1240; blue line/stars; Kienast et al., 2007; Bradtmiller et al., 2010). All lines are B-spline smoothed. Vertical dashed lines delimit relevant climatic periods, and light gray vertical bands highlight the coldest periods of the last 30 kyr. The gray arrow on the $[CO_3^{2-}]$ axis represents the modern water value (67.6 μmol/kg) obtained from GLODAP database (WOCE P19C transect; Tsuchiya & Talley, 1998).

for this respired carbon to accumulate. If this happened, the most noticeable consequences might be, on the one hand, a decrease in seawater $\delta^{13}C$ due to enhanced lighter carbon isotope (^{12}C) release, and on the other hand, a greater CO_2 accumulation in seawater as a product of respiration. Such an increase in seawater $[CO_2]$ would have altered the carbonate system equilibrium, leading to a drop in $[CO_3^{2-}]$ in

order to buffer the change in seawater pH (Sarmiento & Gruber, 2004; Williams & Follows, 2011; Zeebe & Wolf-Gladrow, 2001).

The $[CO_3^{2-}]$ and $\delta^{13}C$ results presented here from ODP1240 are in good agreement with these expectations (Figures 4d and 4e), as well as with a previous study in the area (Doss & Marchitto, 2013), showing lower $\delta^{13}C$ and $[CO_3^{2-}]$ during the late glacial, in parallel with reduced radiocarbon ventilation, and an increase in all of these parameters across the deglaciation. Interestingly, when the modern $[CO_3^{2-}]$ value from this area is taken into account, a drop at the late Holocene is inferred. The existence of such $[CO_3^{2-}]$ decrease across the late Holocene has been previously suggested on the basis of sediment composition data and modeling studies (Berelson et al., 1997; Broecker & Peng, 1987). This feature might reflect a restored lower average ocean alkalinity due to enhanced carbonate preservation associated with the release of excess respired carbon from the ocean interior to the atmosphere during deglaciation, which in turn might have helped to maintain the higher CO_2 in the atmosphere during the late Holocene. However, another plausible explanation for the late Holocene-modern value "mismatch" observed in our core might be related to the inherent noise contained in the B/Ca-$\Delta[CO_3^{2-}]$ calibration applied. Indeed, this issue has been observed in previous studies that estimated $[CO_3^{2-}]$ through B/Ca analysis in benthic foraminifera (Allen et al., 2015; Elmore et al., 2015; Yu et al., 2013, 2008). In order to avoid this mismatch, some of these studies opted for applying a correction by subtracting the core top value to each measurement downcore, thus forcing the record to fall on the regression line given by the equation: $[CO_3^{2-}]_{downcore} = [CO_3^{2-}]_{preindustrial} + \Delta(B/Ca)/1.14$, where $\Delta(B/Ca)$ represents the deviation of each downcore sample relative to the core top value (Yu et al., 2008, 2010, 2013, 2016; Yu, Anderson, Jin, et al., 2014). However, in our study, the conventional option of applying the linear correlation from Yu and Elderfield (2007) without correcting for the core top value has been chosen to avoid applying arbitrary offsets to the data set. This issue would call for cautious approach when considering absolute $[CO_3^{2-}]$ values derived from benthic B/Ca analysis and may suggest that relative changes observed downcore might be more robust than intercore or absolute value comparisons. It would also call for a careful interpretation when using data for any further carbonate system calculations.

Another consequence of the hypothetical increase in respired carbon due to a longer residence time of deep water during the LGM would be a drop in $[O_2]$, as microorganisms consume O_2 during respiration of organic matter. Following reformulations of the traditional Redfield ratios of remineralized organic matter (Redfield et al., 1963), the release of 117 CO_2 molecules consumes 170 molecules of O_2 (Anderson & Sarmiento, 1994). Our U/Ca$_C$ results show the expected depletion in O_2 if the respired carbon content of the ocean interior was indeed higher at the LGM compared to the Holocene (Figure 4f). Moreover, our qualitative relative oxygenation changes indicated by U/Ca$_C$ estimates support previous measurements of authigenic uranium (aU) in core ME0005-24JC (recovered from nominally the same location as Site 1240; Kienast et al., 2007) showing a similar trend, characterized by higher aU (i.e., lower O_2) during the glacial compared to the Holocene (Bradtmiller et al., 2010; Kienast et al., 2007) (Figure 4f).

Thus, all records presented here, that is, $[CO_3^{2-}]$, $\delta^{13}C$, and oxygenation proxies, are in good agreement with the deep radiocarbon ventilation in the EEP and lend support to the hypothesis of a higher efficiency of the biological pump during the LGM due to changes in its leakiness. In the same way, all of these records are in reasonably close agreement through deglaciation, increasing as the deep EEP gets better ventilated at the onset of the last termination. Despite this general agreement, it is interesting to note that both oxygenation proxies, aU and U/Ca$_C$, do not change synchronously with the rest of the proxies at the beginning of the deglaciation, but later at the termination. A plausible explanation for this apparent mismatch might rely on a decoupling of pore water and deep water chemistry, for example, due to a productivity pulse between ~17 and 14 kyr (e.g., Calvo et al., 2011) that would have depleted O_2 in the pore fluids of the sediment (which the oxygenation proxies would record), even after the radiocarbon ventilation and carbonate saturation of the ambient deep water started to increase. Taken together, all the records presented here point to the deep EEP as a plausible contributor to the decreased atmospheric CO_2 during the LGM, by storing more respired carbon at the expense of the surface ocean and atmospheric carbon inventories, that was posteriorly released during the deglaciation once the ocean interior got better ventilated.

A different interpretation based on similar glacial-interglacial $\Delta[CO_3^{2-}]$ changes, also from the Panama Basin, has been proposed by Doss and Marchitto (2013). This study suggests that the observed glacial $\Delta[CO_3^{2-}]$ difference found between a sediment core located at the sill depth and sediment cores located deeper in the

basin are indicative of an increase in the export production during the last glacial. While we do not discard this possibility, which must eventually be tested against other evidence for increased export production during the last glacial period, we propose that it must have acted in addition to a decrease in ocean ventilation, as indicated by our combined proxy results, including radiocarbon ventilation ages. Below we discuss the available evidence for other possible contributions to the apparent increase in the respired carbon content of the deep EEP, including more direct nutrient-based indicators of export production.

4.2. Export Production as a Complementary Mechanism for a Higher Biological Pump Efficiency in the EEP

An increase in the strength of the biological pump (i.e., export production rates) could have operated on the glacial atmospheric CO_2 drawdown independently of, or in addition to, contributions from changes in ocean ventilation constrained using radiocarbon measurements. The glacial changes observed in deep ocean $[CO_3^{2-}]$, $\delta^{13}C$, and oxygenation records from ODP1240, described in the previous subsection, might indeed be compatible with an increase in surface productivity over the LGM. Thus, a larger flux of organic matter to the deep ocean in this area might have contributed to the observed drop in $[CO_3^{2-}]$ and $\delta^{13}C$, as a consequence of higher levels of carbon respiration that would have also increased the release of respired CO_2 to deep water and the consumption of dissolved O_2.

The documented increase in dust-borne iron delivery to the iron-limited low-latitude Pacific Ocean at the last glacial period (McGee et al., 2007) has led to a number of investigations into a potential increase in surface productivity over this period, however, with ambiguous results. On the one hand, lower opal $\delta^{30}Si$ content in ODP1240 as a proxy for the relative utilization of silica during the glacial has been interpreted as an indication of a decline in the Si:C uptake ratio by diatoms due to an iron-replete glacial ocean, which would be compatible with the assumption of higher productivity over this period (Pichevin et al., 2009). Similarly, nitrogen isotopes ($\delta^{15}N$) from bulk sediments in ODP1240 core, once they are corrected for denitrification effects typical of the Central American margin, showed higher values over the LGM compared to the Holocene suggesting higher local nutrient consumption consistent with higher surface productivity over the LGM (Robinson et al., 2009). At the same time, higher abundances of organic biomarkers (alkenones and brassicasterol) have been shown in the same core during the LGM, as compared to the present (Calvo et al., 2011). However, these inferences are contradicted by other studies that do not support the proposed increase in the strength of the biological pump in the EEP as a mechanism for the atmospheric CO_2 drawdown during the LGM (Bradtmiller et al., 2006; Kienast et al., 2006). More recently, for instance, Winckler et al. (2016) reported excess Ba and opal fluxes obtained from sediment cores located along the equatorial Pacific, which do indicate higher productivity in this area (stimulated by an increased Fe supply by upwelling rather than by dust deposition), but with peak export occurring during deglaciation rather than over the LGM. Moreover, Costa et al. (2016) suggested that the glacial dust supply to the equatorial Pacific exerted a negligible effect on surface productivity, arguing that the major nutrient supply with Southern Ocean origin was actually reduced as nutrients were mostly consumed in the Subantartic Zone.

An increase in organic carbon (C_{org}) accumulation rates in the EEP over the LGM has been documented in core ODP1240 (Pichevin et al., 2009), as well as in the nearby core P6 (Pedersen, 1983). Such higher C_{org} accumulation might have been the result of an increase in surface productivity and also the result of better preservation of the organic matter due to lower oxygen content in the deep ocean at that time. Thus, in light of the fact that existing proxy reconstructions can neither corroborate nor rule out unequivocally an increase in EEP surface productivity over the LGM, two key questions remain: was the observed increase in the biological pump efficiency in the glacial EEP mainly due to changes in ocean circulation, or changes in the carbon export production in this area; how much did the proposed increase in organic carbon export production affect carbon storage in the deep ocean? Arguably, these questions cannot be fully resolved without accurate quantitative estimates of export production and deep ocean apparent oxygen utilization changes. Nevertheless, it is clear at least that ocean ventilation changes made some contribution, though only qualitative conclusions, such as those drawn above, are possible at present.

4.3. Carbonate Seafloor Dissolution as a Potential Counteracting Mechanism for $[CO_3^{2-}]$ EEP Changes

A decrease in deep ocean ventilation along with a potential increase in carbon export production in the EEP at the LGM are therefore proposed as the mechanisms responsible for the decrease in deep $[CO_3^{2-}]$, $\delta^{13}C$,
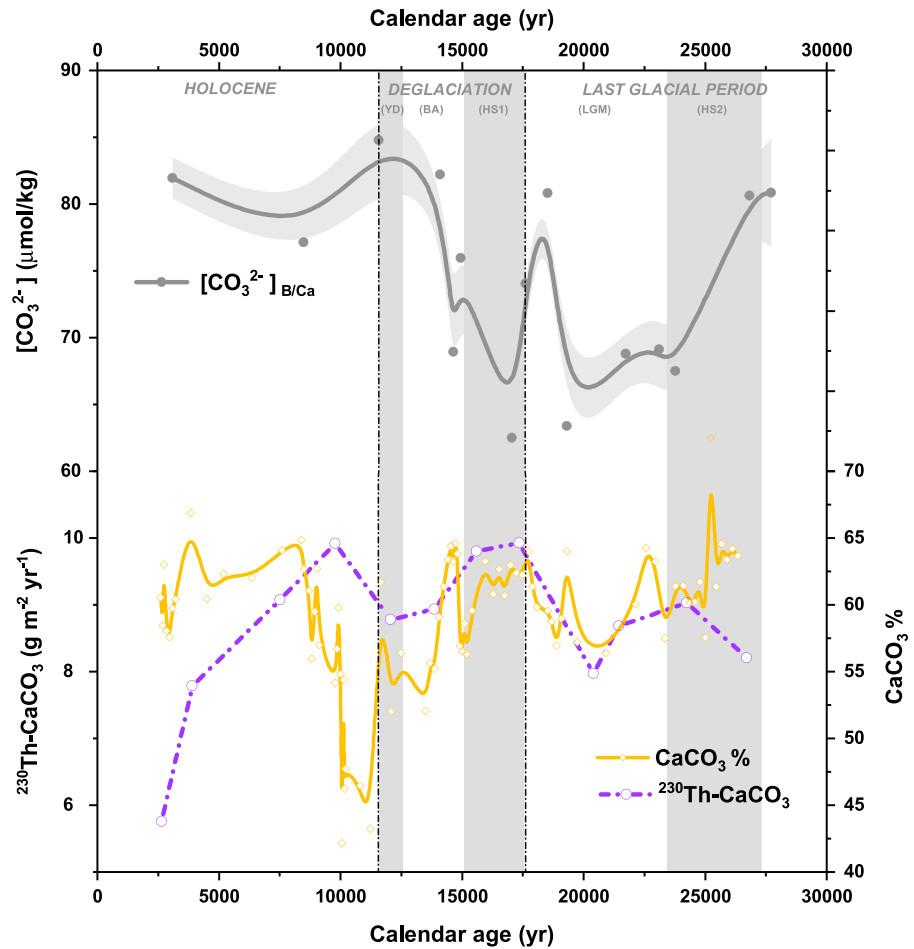
Figure 5. Carbonate chemistry-related records from core ODP1240 across the past 30 kyr. (top) [CO₃²⁻]$_{B/Ca-based}$ (gray line/dots; this study). (bottom) ^{230}Th-CaCO₃ and CaCO₃% (purple dashed line/open dots and yellow line/open diamonds, respectively; Pichevin et al., 2009). Vertical dashed lines delimit relevant climatic periods, and light gray vertical bands highlight the coldest periods of the last 30 kyr.

and oxygenation observed in this area. The action of any of these mechanisms (alone or together) might be expected, in principle, to achieve a relatively large [CO₃²⁻] glacial-Holocene difference. For example, spatial correlations of radiocarbon and [CO₃²⁻] in the modern deep ocean would predict a change of ~ −37 μmol/kg for the ~960 ^{14}C yr increase in deep water radiocarbon ventilation observed in ODP1240 at the LGM relative to the modern ocean (Key et al., 2004). However, the results from this study indicate only a small [CO₃²⁻] change between these two periods (~9 μmol/kg), suggesting that a counteracting mechanism, such as seafloor respiratory calcite dissolution, might have also played a role: when carbonate dissolves in seawater, both [CO₃²⁻] and ALK increase (Broecker & Peng, 1989; Zeebe & Wolf-Gladrow, 2001). If this was the case, a decrease in the CaCO₃ content in sediments might be initially expected. However, CaCO₃% from ODP1240 indicates little change between 25 and 15 kyr (Figure 5). Furthermore, the possibility of an increase in the calcium carbonate export production rates as a masking mechanism for the expected CaCO₃% drop seems not to be supported by carbonate flux data (expressed as ^{230}Th-CaCO₃) from this area, which also show little change between last glacial and Holocene (Figure 5).

Despite no obvious carbonate dissolution in core ODP1240 being observed during the LGM, it remains possible that [CO₃²⁻] was added to deep waters bathing the EEP through carbonate dissolution elsewhere in the Pacific (Anderson et al., 2008). Indeed, similarly small [CO₃²⁻] differences between LGM-Holocene/modern have also been reported in other areas from the Pacific Ocean (Allen et al., 2015; Doss & Marchitto, 2013; Elmore et al., 2015; Yu et al., 2010), and this has been generally attributed to the large buffering capacity of
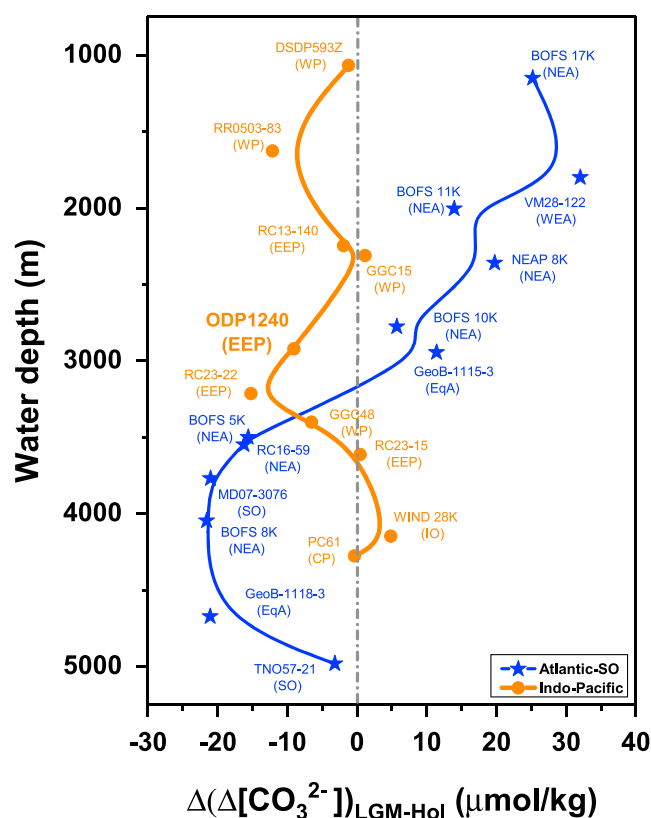
Figure 6. Deep water $[CO_3^{2-}]$ offset between LGM (~18–23 kyr) and Holocene/modern (~0–8 kyr) from several Atlantic/Southern Ocean (in blue) and Indo-Pacific Ocean (in orange) sediment cores. DSDP593Z (Elmore et al., 2015); RR0503-83 (Allen et al., 2015); MW91-9 GGC15, MW91-9 GGC48, WIND 28K, and VM28-122 (Yu et al., 2010); TTNO13 PC61 (Yu et al., 2013); BOFS and NEAP cores (Yu et al., 2008; Yu & Elderfield, 2007); RC13-140, RC23-22, and RC23-15 (Doss & Marchitto, 2013); RC16-59 (Broecker et al., 2015); GeoB cores (Raitzsch et al., 2011); MD07-3076 (Gottschalk et al., 2015); TN057-21 (Yu, Anderson, Jin, et al., 2014); and ODP1240 (this study, highlighted in bold). WP: western Pacific; EEP: Eastern Equatorial Pacific; CP: central Pacific; NEA: North East Atlantic; WEA: western equatorial Pacific; EqA: equatorial Atlantic; SO: Southern Ocean; IO: Indian Ocean.

carbonate sediments in this basin (Allen et al., 2015; Yu et al., 2010, 2013). In Figure 6, a compilation of the averaged $\Delta[CO_3^{2-}]$ offsets between the LGM (~18–23 kyr) and the late Holocene (~0–8 kyr) ($\Delta(\Delta[CO_3^{2-}])_{LGM-Hol}$) from these studies shows the consistency among the Indo-Pacific sites with variations of only ~5 μmol/kg between these two periods (orange line in Figure 6). By restricting the comparison to LGM-Hol differences, potential biases due to different techniques/calibrations/standards can be avoided, as well as any biases that may arise from assuming constant local $[CO_3^{2-}]_{sat}$ across the deglaciation. Thus, negative values represent lower $\Delta[CO_3^{2-}]$ at the LGM compared to the Holocene, while positive ones represent the opposite. The small LGM-late Holocene difference observed in the Indo-Pacific, in contrast with larger offsets detected within the Atlantic and Southern Oceans (blue line in Figure 6) (Gottschalk et al., 2015; Yu et al., 2008, 2013; Yu, Anderson, Jin, et al., 2014; Yu, Anderson, & Rohling, 2014) still implies lower LGM $\Delta[CO_3^{2-}]$ for the whole Pacific as well as for the Atlantic and Southern Ocean at depths greater than ~2,500 m water depth. However, the $\Delta(\Delta[CO_3^{2-}])_{LGM-Hol}$ changes present a noticeable difference between basins above ~2,500 m water depth. This might point to the accumulation of respired DIC (i.e., not equilibrated with the atmosphere) in the Pacific, Southern Ocean, and Atlantic >2,500 m during the last glacial, and the maintenance of "equilibrium" DIC (Ito & Follows, 2013) in Atlantic water masses shallower than ~2,500 m. The shallow Atlantic would thus have responded more closely to changes in the atmosphere, such that lower atmospheric CO_2 would be directly manifested as higher LGM $[CO_3^{2-}]$ (Hodell et al., 2001; Yu et al., 2008). In this situation, seafloor $CaCO_3$ not only might have "buffered" glacial $[CO_3^{2-}]$ changes in the EEP (without affecting $\delta^{13}C$ significantly) but also might have played a role in the atmospheric CO_2 drawdown during the LGM by contributing to increased average ocean alkalinity via $[CO_3^{2-}]$ supply to the ocean (Keir, 1995; Sigman & Boyle, 2000). This would have further reinforced the effects of a higher biological pump efficiency achieved by circulation changes, and perhaps also by surface productivity changes.

Interestingly, calculations based on the modern $\delta^{13}C$-$[CO_3^{2-}]$ relationship in the Panama Basin suggest that the observed glacial-interglacial $\delta^{13}C$ difference is compatible with the observed glacial-interglacial offset in $[CO_3^{2-}]$ (when a whole ocean glacial-interglacial $\delta^{13}C$ change of ~0.3‰ is assumed, due to terrestrial carbon release), which would imply no further $[CO_3^{2-}]$ addition from calcite dissolution (Doss & Marchitto, 2013). Following the calculations of Doss and Marchitto (2013), a 10 μmol/kg $[CO_3^{2-}]$ glacial-interglacial drop would achieve a 30 μmol/kg DIC increase, which in turn would produce a ~0.26‰ change in $\delta^{13}C$ due to respired carbon addition. If a whole ocean change of ~0.3‰ (Peterson et al., 2014) is assumed to have occurred exclusively due to terrestrial carbon release (Shackleton, 1977), a total change of ~0.56‰ would therefore be expected, which is not very far off the results of Doss and Marchitto (2013) and our observed glacial-interglacial $\delta^{13}C$ difference of 0.4 ± 0.06‰. However, it is notable that the observed global average glacial-interglacial $\delta^{13}C$ change of ~0.3‰ corresponds to a global average radiocarbon ventilation age change of perhaps ~689 ^{14}C yr (Skinner et al., 2017), which raises the question of how this average change can be partitioned into a "terrestrial carbon component" and a "ventilation/respired carbon component." Until this issue is resolved, along with the related issue of how subaerial volcanism changed across the last glacial period (Broecker et al., 2015), the possibility remains that much of the full glacial-interglacial $\delta^{13}C$ difference observed in ODP1240 was achieved by respired carbon addition, implying that a bigger drop in $[CO_3^{2-}]$ would be expected. This, in turn, would point to an additional process that would have counterbalanced the addition of $[CO_3^{2-}]$ from organic carbon respiration, such as $CaCO_3$ dissolution.

5. Conclusions

In this study, an increase in the biological pump efficiency over the LGM through a decrease in its leakiness has been investigated in the EEP as a mechanism for the glacial atmospheric CO_2 drawdown. The change in $[CO_3^{2-}]$, $\delta^{13}C$ and oxygenation proxies inferred in this study support this idea by presenting lower values in the EEP at the LGM compared to the late Holocene. However, the decrease in $[CO_3^{2-}]$ in this area is relatively small, suggesting that these mechanisms were not the only ones operating or indeed contributing to the drop in glacial atmospheric CO_2. This has also been observed in other Pacific $[CO_3^{2-}]$ records and has been suggested to be a consequence of larger carbonate dissolution over the LGM in this basin. Thus, respiratory calcite dissolution not only might explain the relatively small change in deep ocean $[CO_3^{2-}]$ between the glacial and late Holocene periods but also would have likely and directly contributed to the glacial atmospheric CO_2 decrease by increasing the ocean average ALK and therefore decreasing the surface ocean pCO$_2$, thus allowing the surface ocean to take up more CO_2. In conclusion, the deep EEP, and probably much of the wider deep Pacific, likely sequestered a significant amount of atmospheric CO_2 during the LGM, specifically due to a more efficient biological carbon pump caused by lower ventilation rates (and potentially also enhanced export production) and also due to an increase in average ocean alkalinity by respiratory calcite dissolution. However, a comparison with $\delta^{13}C$ data raises interesting questions regarding the relative contributions to the global marine carbon inventory during the last glacial period, from changes in deep ocean ventilation, export production, carbonate dissolution, terrestrial carbon release, and indeed volcanism. Further investigation in other basins using a "biogeochemical fingerprinting" approach as applied in this study would help to address these questions, for example, through better constraints on global average ocean chemistry changes at the LGM, which in turn would allow for a more accurate quantification of carbonate dissolution effects and marine CO_2 sequestration over this period.

References

Allen, K. A., Sikes, E. L., Hönisch, B., Elmore, A. C., Guilderson, T. P., Rosenthal, Y., & Anderson, R. F. (2015). Southwest Pacific deep water carbonate chemistry linked to high southern latitude climate and atmospheric CO_2 during the Last Glacial Termination. *Quaternary Science Reviews*, 122, 180–191. https://doi.org/10.1016/j.quascirev.2015.05.007

Anderson, L. A., & Sarmiento, J. L. (1994). Redfield ratios of remineralization determined by nutrient data analysis. *Global Biogeochemical Cycles*, 8(1), 65–80. https://doi.org/10.1029/93GB03318

Anderson, R. F., Fleisher, M. Q., Lao, Y., & Winckler, G. (2008). Modern CaCO$_3$ preservation in equatorial Pacific sediments in the context of late-Pleistocene glacial cycles. *Marine Chemistry*, 111(1-2), 30–46. https://doi.org/10.1016/j.marchem.2007.11.011

Archer, D. (1991). Equatorial Pacific calcite preservation cycles: Production or dissolution? *Paleoceanography*, 6(5), 561–571. https://doi.org/10.1029/91PA01630

Archer, D. (1996). A data-driven model of the global calcite lysocline. *Global Biogeochemical Cycles*, 10(3), 511–526. https://doi.org/10.1029/96GB01521

Archer, D., & Maier-Reimer, E. (1994). Effect of deep-sea sedimentary calcite preservation on atmospheric CO_2 concentration. *Nature*, 367(6460), 260–263. https://doi.org/10.1038/367260a0

Berelson, W. M., Anderson, R. F., Dymond, J., Demaster, D., Hammond, D. E., Collier, R., … Stephens, M. (1997). Biogenic budgets of particle rain, benthic remineralization and sediment accumulation in the equatorial Pacific. *Deep-Sea Research Part II: Topical Studies in Oceanography*, 44(9–10), 2251–2282. https://doi.org/10.1016/S0967-0645(97)00030-1

Boiteau, R., Greaves, M., & Elderfield, H. (2012). Authigenic uranium in foraminiferal coatings: A proxy for ocean redox chemistry. *Paleoceanography*, 27, PA3227. https://doi.org/10.1029/2012PA002335

Bolton, A., Baker, J. A., Dunbar, G. B., Carter, L., Smith, E. G. C., & Neil, H. L. (2011). Environmental versus biological controls on Mg/Ca variability in *Globigerinoides ruber* (white) from core top and plankton tow samples in the southwest Pacific Ocean. *Paleoceanography*, 26, PA2219. https://doi.org/10.1029/2010PA001924

Boyle, E. A. (1983). Manganese carbonate overgrowths on foraminifera tests. *Geochimica et Cosmochimica Acta*, 47(10), 1815–1819. https://doi.org/10.1016/0016-7037(83)90029-7

Bradtmiller, L., Anderson, R. F., Fleisher, M. Q., & Burk, C. (2006). Diatom productivity in the equatorial Pacific Ocean from the last glacial period to the present: A test of the silicic acid leakage hypothesis. *Paleoceanography*, 21, PA4201. https://doi.org/10.1029/2006PA001282

Bradtmiller, L., Anderson, R. F., Sachs, J. P., & Fleisher, M. Q. (2010). A deeper respired carbon pool in the glacial equatorial Pacific Ocean. *Earth and Planetary Science Letters*, 299(3-4), 417–425. https://doi.org/10.1016/j.epsl.2010.09.022

Broecker, W. S., & Peng, T. -H. (1987). The role of CaCO$_3$ compensation in the glacial to interglacial atmospheric CO_2 change. *Global Biogeochemical Cycles*, 1(1), 15–29. https://doi.org/10.1029/GB001i001p00015

Broecker, W. S., & Peng, T.-H. (1989). The cause of the glacial to interglacial atmospheric CO_2 change: A polar alkalinity hypothesis. *Global Biogeochemical Cycles*, 3(3), 215–239. https://doi.org/10.1029/GB003i003p00215

Broecker, W. S., Yu, J., & Putnam, A. E. (2015). Two contributors to the glacial CO_2 decline. *Earth and Planetary Science Letters*, 429, 191–196. https://doi.org/10.1016/j.epsl.2015.07.019

Brown, R. E., Anderson, L. D., Thomas, E., & Zachos, J. (2011). A core-top calibration of B/Ca in the benthic foraminifers *Nuttallides umbonifera* and *Oridorsalis umbonatus*: A proxy for Cenozoic bottom water carbonate saturation. *Earth and Planetary Science Letters*, 310(3-4), 360–368. https://doi.org/10.1016/j.epsl.2011.08.023

Burke, A., & Robinson, L. (2012). The Southern Ocean's role in carbon exchange during the last deglaciation. *Science*, 335(6068), 557–561. https://doi.org/10.1126/science.1208163

Calvo, E., Pelejero, C., Pena, L. D., Cacho, I., & Logan, G. A. (2011). Eastern equatorial pacific productivity and related-CO_2 changes since the last glacial period. *Proceedings of the National Academy of Sciences of the United States of America*, *108*(14), 5537–5541. https://doi.org/10.1073/pnas.1009761108

Cochran, J. K., Carey, A. E., Sholkovitz, E., & Surprenant, L. (1986). The geochemistry of uranium and thorium in coastal marine sediments and sediment pore waters. *Geochimica et Cosmochimica Acta*, *50*(5), 663–680. https://doi.org/10.1016/0016-7037(86)90344-3

Costa, K. M., McManus, J. F., Anderson, R. F., Ren, H., Sigman, D. M., Winckler, G., … Ravelo, A. C. (2016). No iron fertilization in the equatorial Pacific Ocean during the last ice age. *Nature*, *529*(7587), 519–522. https://doi.org/10.1038/nature16453

de la Fuente, M., Skinner, L., Calvo, E., Pelejero, C., & Cacho, I. (2015). Increased reservoir ages and poorly ventilated deep waters inferred in the glacial Eastern Equatorial Pacific. *Nature Communications*, *6*, 7420. https://doi.org/10.1038/ncomms8420

Dickson, A. G., & Millero, F. J. (1987). A comparison of the equilibrium constants for the dissociation of carbonic acid in seawater media. *Deep-Sea Research Part A: Oceanographic Research Papers*, *34*(10), 1733–1743. https://doi.org/10.1016/0198-0149(87)90021-5

Doss, W., & Marchitto, T. M. (2013). Glacial deep ocean sequestration of CO_2 driven by the eastern equatorial Pacific biologic pump. *Earth and Planetary Science Letters*, *377-378*, 43–54. https://doi.org/10.1016/j.epsl.2013.07.019

Eggins, S., Kinsley, L. P. J., & Shelley, J. M. G. (1998). Deposition and element fractionation processes during atmospheric pressure laser sampling for analysis by ICP-MS. *Applied Surface Science*, *127-129*, 278–286. https://doi.org/10.1016/S0169-4332(97)00643-0

Elmore, A. C., McClymont, E. L., Elderfield, H., Kender, S., Cook, M. R., Leng, M. J., … Misra, S. (2015). Antarctic Intermediate Water properties since 400 ka recorded in infaunal (*Uvigerina peregrina*) and epifaunal (*Planulina wuellerstorfi*) benthic foraminifera. *Earth and Planetary Science Letters*, *428*, 193–203. https://doi.org/10.1016/j.epsl.2015.07.013

Evans, D., & Müller, W. (2013). LA-ICPMS elemental imaging of complex discontinuous carbonates: An example using large benthic foraminifera. *Journal of Analytical Atomic Spectrometry*, *28*(7), 1039. https://doi.org/10.1039/c3ja50053e

Evans, D., Rehemat, B., Stoll, H., & Müller, W. (2015). LA-ICPMS Ba/Ca analyses of planktic foraminifera from the Bay of Bengal: Implications for late Pleistocene orbital control on monsoon freshwater flux. *Geochemistry, Geophysics, Geosystems*, *16*(8), 2598–2618. https://doi.org/10.1002/2015GC005822

Flückiger, J., Monnin, E., Stauffer, B., Schwander, J., & Stocker, T. F. (2002). High-resolution Holocene N_2O ice core record and its relationship with CH_4 and CO_2. *Global Biogeochemical Cycles*, *16*(1), 10-1–10-8. https://doi.org/10.1029/2001GB001417

Gottschalk, J., Skinner, L., Lippold, J., Vogel, H., Frank, N., Jaccard, S., & Waelbroeck, C. (2016). Biological and physical controls in the Southern Ocean on past millennial-scale atmospheric CO_2 changes. *Nature Communications*, *7*. https://doi.org/10.1038/ncomms11539

Gottschalk, J., Skinner, L., Misra, S., Waelbroeck, C., Menviel, L., & Timmermann, A. (2015). Abrupt changes in the southern extent of North Atlantic Deep Water during Dansgaard–Oeschger events. *Nature Geoscience*, *8*(12), 950–954. https://doi.org/10.1038/ngeo2558

Hodell, D. A., Charles, C. D., & Sierro, F. (2001). Late Pleistocene evolution of the ocean's carbonate system. *Earth and Planetary Science Letters*, *192*(2), 109–124. https://doi.org/10.1016/S0012-821X(01)00430-7

Ito, T., & Follows, M. J. (2013). Air-sea disequilibrium of carbon dioxide enhances the biological carbon sequestration in the Southern Ocean. *Global Biogeochemical Cycles*, *27*(4), 1129–1138. https://doi.org/10.1002/2013GB004682

Jaccard, S., Galbraith, E., Martínez-Garcia, A., & Anderson, R. F. (2016). Covariation of deep Southern Ocean oxygenation and atmospheric CO_2 through the last ice age. *Nature*, *530*(7589), 207–210. https://doi.org/10.1038/nature16514

Jochum, K. P., Stoll, B., Herwig, K., Willbold, M., Hofmann, A. W., Amini, M., … Woodhead, J. D. (2006). MPI-DING reference glasses for in situ microanalysis: New reference values for element concentrations and isotope ratios. *Geochemistry, Geophysics, Geosystems*, *7*(2), Q02008. https://doi.org/10.1029/2005GC001060

Jochum, K. P., Weis, U., Stoll, B., Kuzmin, D., Yang, Q., Raczek, I., … Enzweiler, J. (2011). Determination of reference values for NIST SRM 610-617 glasses following ISO guidelines. *Geostandards and Geoanalytical Research*, *35*(4), 397–429. https://doi.org/10.1111/j.1751-908X.2011.00120.x

Keir, R. S. (1995). Is there a component of Pleistocene CO_2 change associated with carbonate dissolution cycles? *Paleoceanography*, *10*(5), 871–880. https://doi.org/10.1029/95PA02177

Kessler, W. (2006). The circulation of the eastern tropical Pacific: A review. *Progress in Oceanography*, *69*(2-4), 181–217. https://doi.org/10.1016/j.pocean.2006.03.009

Key, R. M., Kozyr, A., Sabine, C. L., Lee, K., Wanninkhof, R., Bullister, J. L., … Peng, T.-H. (2004). A global ocean carbon climatology: Results from Global Data Analysis Project (GLODAP). *Global Biogeochemical Cycles*, *18*, GB4031. https://doi.org/10.1029/2004GB002247

Kienast, M., Kienast, S., Calvert, S. E., Eglinton, T. I., Mollenhauer, G., François, R., & Mix, A. (2006). Eastern Pacific cooling and Atlantic overturning circulation during the last deglaciation. *Nature*, *443*(7113), 846–849. https://doi.org/10.1038/nature05222

Kienast, S., Kienast, M., Mix, A., Calvert, S. E., & François, R. (2007). Thorium-230 normalized particle flux and sediment focusing in the Panama Basin region during the last 30,000 years. *Paleoceanography*, *22*, PA2213. https://doi.org/10.1029/2006PA001357

Kohfeld, K. E., & Ridgwell, A. (2009). Glacial-interglacial variability in atmospheric CO_2. In C. L. Quéré & E. S. Saltzman (Eds.), *Surface ocean-lower atmosphere processes* (Vol. 187, pp. 251–286). Washington, DC: American Geophysical Union. https://doi.org/10.1029/2008GM000845

Kwon, E. Y., Primeau, F., & Sarmiento, J. L. (2009). The impact of remineralization depth on the air–sea carbon balance. *Nature Geoscience*, *2*(9), 630–635. https://doi.org/10.1038/ngeo612

Langmuir, D. (1978). Uranium solution-mineral equilibria at low temperatures with applications to sedimentary ore deposits. *Geochimica et Cosmochimica Acta*, *42*(6), 547–569. https://doi.org/10.1016/0016-7037(78)90001-7

Lemieux-Dudon, B., Blayo, E., Petit, J.-R., Waelbroeck, C., Svensson, A., Ritz, C., … Parrenin, F. (2010). Consistent dating for Antarctic and Greenland ice cores. *Quaternary Science Reviews*, *29*(1-2), 8–20. https://doi.org/10.1016/j.quascirev.2009.11.010

Lewis, E., Wallace, D., & Allison, L. J. (1998). Program developed for CO_2 system calculations, Carbon Dioxide Information Analysis Center, managed by Lockheed Martin Energy Research Corporation for the US Department of Energy.

Longerich, H. P., Jackson, S. E., & Günther, D. (1996). Laser ablation inductively coupled plasma mass spectrometric transient signal data acquisition and analyte concentration calculation. *Journal of Analytical Atomic Spectrometry*, *11*(9), 899–904. https://doi.org/10.1039/JA9961100899

Mantyla, A. W., & Reid, J. L. (1983). Abyssal characteristics of the World Ocean waters. *Deep-Sea Research Part A: Oceanographic Research Papers*, *30*(8), 805–833. https://doi.org/10.1016/0198-0149(83)90002-X

Marr, J. P., Baker, J. A., Carter, L., Allan, A. S. R., Dunbar, G. B., & Bostock, H. C. (2011). Ecological and temperature controls on Mg/Ca ratios of *Globigerina bulloides* from the southwest Pacific Ocean. *Paleoceanography*, *26*, PA2209. https://doi.org/10.1029/2010PA002059

Martínez-Garcia, A., Sigman, D. M., Ren, H., Anderson, R. F., Straub, M., Hodell, D. A., … Haug, G. H. (2014). Iron fertilization of the Subantarctic ocean during the last ice age. *Science*, *343*(6177), 1347–1350. https://doi.org/10.1126/science.1246848

McGee, D., Marcantonio, F., & Lynch-Stieglitz, J. (2007). Deglacial changes in dust flux in the eastern equatorial Pacific. *Earth and Planetary Science Letters*, *257*(1-2), 215–230. https://doi.org/10.1016/j.epsl.2007.02.033

Mehrbach, C., Culberson, C. H., Hawley, J. E., & Pytowicz, R. M. (1973). Measurements of the apparent dissociation constants of carbonic acid in seawater at atmospheric pressure. *Limnology and Oceanography*, *18*(6), 897–907. https://doi.org/10.4319/lo.1973.18.6.0897

Monnin, E., Indermühle, A., Dällenbach, A., Flückiger, J., Stauffer, B., Stocker, T. F., … Barnola, J. (2001). Atmospheric CO_2 concentrations over the last glacial termination. *Science*, *291*(5501), 112–114. https://doi.org/10.1126/science.291.5501.112

Morford, J. L., & Emerson, S. (1999). The geochemistry of redox sensitive trace metals in sediments. *Geochimica et Cosmochimica Acta*, *63*(11-12), 1735–1750. https://doi.org/10.1016/S0016-7037(99)00126-X

Müller, W., & Fietzke, J. (2016). The role of LA-ICP-MS in palaeoclimate research. *Elements*, *12*(5), 329–334. https://doi.org/10.2113/gselements.12.5.329

Müller, W., Shelley, J. M. G., Miller, P., & Broude, S. (2009). Initial performance metrics of a new custom-designed ArF excimer LA-ICPMS system coupled to a two-volume laser-ablation cell. *Journal of Analytical Atomic Spectrometry*, *24*(2), 209–214. https://doi.org/10.1039/b805995k

Pedersen, T. F. (1983). Increased productivity in the eastern equatorial Pacific during the last glacial maximum (19,000 to 14,000 yr B.P). *Geology*, *11*(1), 16–19. https://doi.org/10.1130/0091-7613(1983)11%3C16

Peterson, C. D., Lisiecki, L., & Stern, J. V. (2014). Deglacial whole-ocean $\delta^{13}C$ change estimated from 480 benthic foraminiferal records. *Paleoceanography*, *29*, 549–563. https://doi.org/10.1002/2013PA002552

Pichevin, L., Reynolds, B. C., Ganeshram, R. S., Cacho, I., Pena, L. D., Keefe, K., & Ellam, R. M. (2009). Enhanced carbon pump inferred from relaxation of nutrient limitation in the glacial ocean. *Nature*, *459*(7250), 1114–1117. https://doi.org/10.1038/nature08101

Pierrot, D., Lewis, E., & Wallace, D. W. R. (2006). MS Excel program developed for CO_2 system calculations, ORNL/CDIAC-105a Carbon Dioxide Information Analysis Center, Oak Ridge National Laboratory, US Department of Energy, Oak Ridge, TN.

Rae, J. W. B., Foster, G. L., Schmidt, D. N., & Elliott, T. (2011). Boron isotopes and B/Ca in benthic foraminifera: Proxies for the deep ocean carbonate system. *Earth and Planetary Science Letters*, *302*(3-4), 403–413. https://doi.org/10.1016/j.epsl.2010.12.034

Raitzsch, M., Hathorne, E. C., Kuhnert, H., Groeneveld, J., & Bickert, T. (2011). Modern and late Pleistocene B/Ca ratios of the benthic foraminifer *Planulina wuellerstorfi* determined with laser ablation ICP-MS. *Geology*, *39*(11), 1039–1042. https://doi.org/10.1130/G32009.1

Redfield, A. C., Ketchum, B. H., & Richards, F. A. (1963). The influence of organisms on the composition of sea-water. *The sea*, *2*, 26–77.

Reimer, P. J., Baillie, M. G. L., Bard, E., Bayliss, A., Berk, J., Blackwell, P. G., … Burr, G. S. (2009). IntCal09 and marine09 radiocarbon age calibration curves, 0–50,000 years cal BP. *Radiocarbon*, *51*(04), 1111–1150. https://doi.org/10.1017/S0033822200034202

Robinson, R., Martinez, P., Pena, L. D., & Cacho, I. (2009). Nitrogen isotopic evidence for deglacial changes in nutrient supply in the eastern equatorial Pacific. *Paleoceanography*, *24*, PA4213. https://doi.org/10.1029/2008PA001702

Sarmiento, J. L., & Gruber, N. (2004). *Ocean biogeochemical dynamics*. Princeton, NJ: Princeton University Press.

Schlitzer, R. (2017). Ocean Data View. Retrieved from http://odv.awi.de

Shackleton, N. J. (1977). Carbon-13 in Uvigerina: Tropical rain forest history and the equatorial Pacific carbonate dissolution cycle. In N. R. Andersen & A. Malahoff (Eds.), *The fate of fossil fuel in the oceans* (pp. 401–427). New York: Plenum. https://doi.org/10.1007/978-1-4899-5016-1_22

Siani, G., Michel, E., De Pol-Holz, R., Devries, T., Lamy, F., Carel, M., … Lourantou, A. (2013). Carbon isotope records reveal precise timing of enhanced Southern Ocean upwelling during the last deglaciation. *Nature Communications*, *4*. https://doi.org/10.1038/ncomms3758

Sigman, D. M., & Boyle, E. A. (2000). Glacial/interglacial variations in atmospheric carbon dioxide. *Nature*, *407*(6806), 859–869. https://doi.org/10.1038/35038000

Sigman, D. M., Hain, M. P., & Haug, G. H. (2010). The polar ocean and glacial cycles in atmospheric CO_2 concentration. *Nature Reviews*, *466*(7302), 47–55. https://doi.org/10.1038/nature09149

Sikes, E. L., Samson, C. R., Guilderson, T. P., & Howard, W. R. (2000). Old radiocarbon ages in the southwest Pacific Ocean during the last glacial period and deglaciation. *Nature*, *303*, 555–559.

Skinner, L., Fallon, S. J., Waelbroeck, C., Michel, E., & Barker, S. (2010). Ventilation of the deep Southern Ocean and deglacial CO_2 rise. *Science*, *328*(5982), 1147–1151. https://doi.org/10.1126/science.1183627

Skinner, L., McCave, N. I., Carter, L., Fallon, S. J., Scrivner, A., & Primeau, F. (2015). Reduced ventilation and enhanced magnitude of the deep Pacific carbon pool during the last glacial period. *Earth and Planetary Science Letters*, *411*, 45–52. https://doi.org/10.1016/j.epsl.2014.11.024

Skinner, L. C. L., Primeau, F., Freeman, E., de la Fuente, M., Goodwin, P. A., Gottschalk, J., … Scrivner, A. E. (2017). Radiocarbon constraints on the glacial ocean circulation and its impact on atmospheric CO_2. *Nature Communications*, *8*, 1–10. https://doi.org/10.1038/ncomms16010

Stephens, B. B., & Keeling, R. F. (2000). The influence of Antarctic sea ice on glacial-interglacial CO_2 variations. *Nature*, *404*(6774), 171–174. https://doi.org/10.1038/35004556

Strub, P., Mesías, J., Montecino, V., Rutlant, J., & Salinas, S. (1998). Coastal ocean circulation off western South America, Coastal segment (6,E). In A. R. Robinson & K. H. Brink (Eds.), *The sea* (Vol. 11, pp. 273–314). New York: John Wiley & Sons.

Talley, L. D., Pickard, G. L., Emery, W. J., & Swift, J. H. (2011). *Descriptive physical oceanography: An introduction* (6th ed.). Boston: Elsevier.

Toggweiler, J. R. (1999). Variation of atmospheric CO_2 by ventilation of the ocean's deepest water. *Paleoceanography*, *14*(5), 571–588. https://doi.org/10.1029/1999PA900033

Tsuchiya, M., & Talley, L. D. (1998). A Pacific hydrography section at 88°W: Water-property distribution. *Journal of Geophysical Research*, *103*(C6), 12,899–12,918. https://doi.org/10.1029/97JC03415

Umling, N. E., & Thunell, R. C. (2017). Synchronous deglacial thermocline and deep-water ventilation in the eastern equatorial Pacific. *Nature Communications*, *8*. https://doi.org/10.1038/ncomms14203

Volk, T., & Hoffert, M. I. (1985). Ocean carbon pumps: Analysis of relative strengths and efficiencies in ocean-driven atmospheric CO_2 changes. *Geophysical Monograph Series*, *32*, 99–110.

Williams, R. G., & Follows, M. J. (2011). *Ocean dynamics and the carbon cycle: Principles and mechanisms*. Cambridge, UK: Cambridge University Press. https://doi.org/10.1017/CBO9780511977817

Winckler, G., Anderson, R. F., Jaccard, S., & Marcantonio, F. (2016). Ocean dynamics, not dust, have controlled equatorial Pacific productivity over the past 500,000 years. *Proceedings of the National Academy of Sciences of the United States of America*, *113*(22), 6119–6124. https://doi.org/10.1073/pnas.1600616113

You, Y. (2000). Implications of the deep circulation and ventilation of the Indian Ocean on the renewal mechanism of North Atlantic Deep Water. *Journal of Geophysical Research*, *105*(C10), 23,895–23,926. https://doi.org/10.1029/2000JC900105

Yu, J., Anderson, R. F., Jin, Z., Menviel, L., Zhang, F., Ryerson, F. J., & Rohling, E. J. (2014). Deep South Atlantic carbonate chemistry and increased interocean deep water exchange during last deglaciation. *Quaternary Science Reviews*, *90*, 80–89. https://doi.org/10.1016/j.quascirev.2014.02.018

Yu, J., Anderson, R. F., Jin, Z., Rae, J. W. B., Opdyke, B. N., & Eggins, S. (2013). Responses of the deep ocean carbonate system to carbon reorganization during the Last Glacial–interglacial cycle. *Quaternary Science Reviews*, *76*, 39–52. https://doi.org/10.1016/j.quascirev.2013.06.020

Yu, J., Anderson, R. F., & Rohling, E. J. (2014). Deep ocean carbonate chemistry and glacial-interglacial atmospheric CO_2 changes. *Oceanography*, *27*(1), 16–25. https://doi.org/10.5670/oceanog.2014.04

Yu, J., Broecker, W. S., Elderfield, H., Jin, Z., McManus, J. F., & Zhang, F. (2010). Loss of carbon from the deep sea since the Last Glacial Maximum. *Science*, *330*(6007), 1084–1087. https://doi.org/10.1126/science.1193221

Yu, J., & Elderfield, H. (2007). Benthic foraminiferal B/Ca ratios reflect deep water carbonate saturation state. *Earth and Planetary Science Letters*, *258*(1-2), 73–86. https://doi.org/10.1016/j.epsl.2007.03.025

Yu, J., Elderfield, H., & Piotrowski, A. M. (2008). Seawater carbonate ion-δ^{13}C systematics and application to glacial–interglacial North Atlantic ocean circulation. *Earth and Planetary Science Letters*, *271*(1-4), 209–220. https://doi.org/10.1016/j.epsl.2008.04.010

Yu, J., Menviel, L., Jin, Z. D., Thornalley, D. J. R., Barker, S., Marino, G., … Broecker, W. S. (2016). Sequestration of carbon in the deep Atlantic during the last glaciation. *Nature Geoscience*, *9*(4), 319–324. https://doi.org/10.1038/ngeo2657

Zeebe, R., & Wolf-Gladrow, D. A. (2001). *CO_2 in seawater: Equilibrium, kinetics, isotopes, Elsevier Oceanography Series, 65* (pp. 346). Amsterdam, Netherlands.